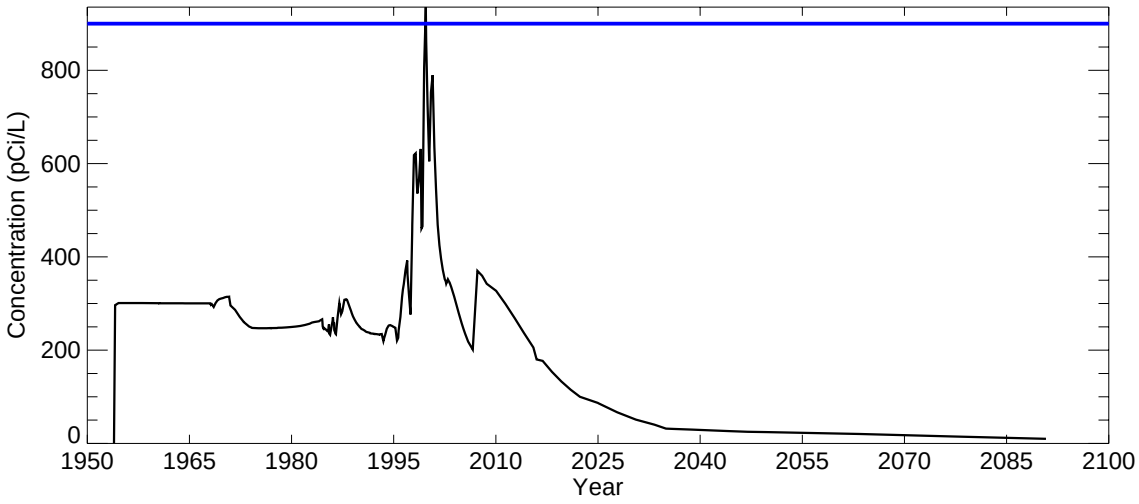

Figure A-9-35. Tc-99 peak aquifer concentrations (pCi/L) (SRPA MCL = blue line, model predicted=black line).

A-9.3.7 U-234

The sources of U-234 in the vadose zone, listed in order of decreasing magnitude, are (1) OU 3-13 soil sites (0.14 Ci), (2) the tank farm at 0.095 Ci, (3) service waste ponds at 0.040 Ci, and (4) CPP-3 injection well failure at 0.011 Ci. The amount of U-234 released directly into the aquifer due to the injection well failure was 0.13 Ci. An early conservative estimate of the OU 3-14 U-234 source term was mistakenly used for the U-234 simulation. The estimate for U-234 developed in Section 5 of the main document was smaller. The model was not rerun with the smaller value because the source term was conservatively larger and the peak simulated U-234 aquifer concentration was several orders of magnitude below the Snake River Plain Aquifer MCL. The Snake River Plain Aquifer MCL for uranium is based on toxicity, and the simulated impact of U-234 to groundwater is being evaluated based on the Snake River Plain Aquifer MCL of 0.03 mg/L.

A-9.3.7.1 Vadose Zone U-234 Simulation Results

Figure A-9-36 presents the peak vadose zone concentrations (excluding the tank farm submodel area) through time and Figure A-9-37 illustrates the U-234 mass flux into the aquifer. Horizontal and vertical concentration plots are not presented because the peak concentrations were always nearly two orders of magnitude below the Snake River Plain Aquifer MCL of 0.03 mg/L.

The purpose of reprocessing spent nuclear fuel was to recover uranium. The process was very efficient and the amount of uranium entering the reprocessing waste stream was small compared to the other radionuclides. The peak vadose zone concentration (excluding the tank farm submodel area) was 8.27e-4 mg/L in 1990 and corresponds to near-surface OU 3-13 soil sources.

A-9.3.7.2 Aquifer U-234 Simulation Results

Figure A-9-38 presents the peak aquifer concentrations through time. The peak aquifer U-234 concentration was 5.36e-7 mg/L in 1958 and is the result of the CPP-3 injection well. Horizontal aquifer concentration contour plots are not presented because the simulated U-234 concentrations were always several orders of magnitude below the Snake River Plain Aquifer MCL.

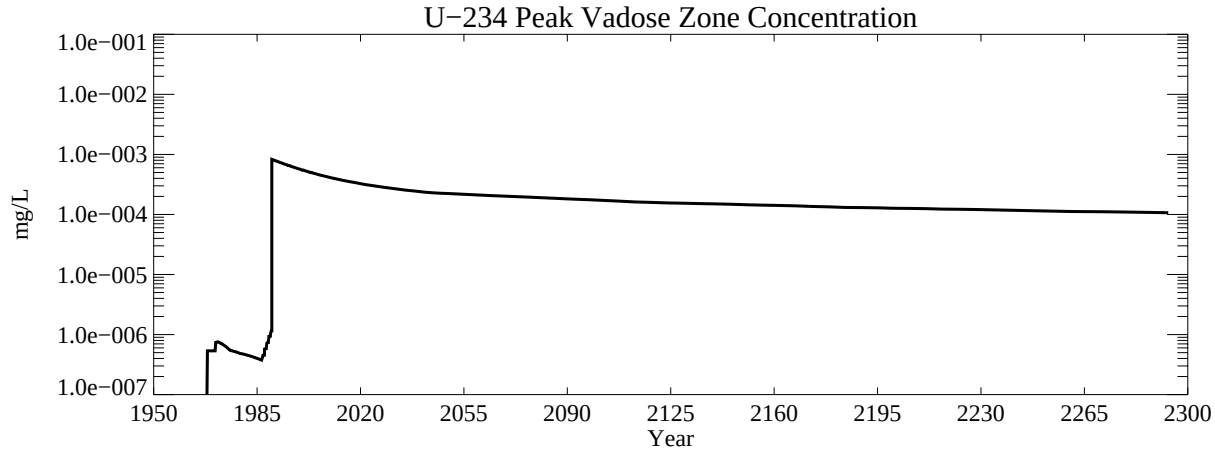

Figure A-9-36. U-234 peak vadose zone concentrations excluding tank farm submodel area (mg/L).

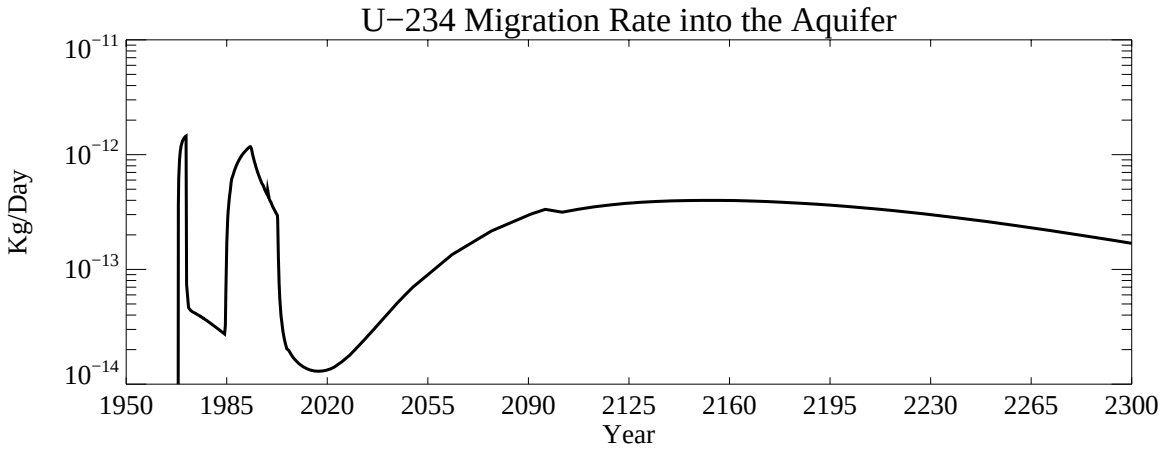

Figure A-9-37. U-234 mass flux into the aquifer (kg/day).

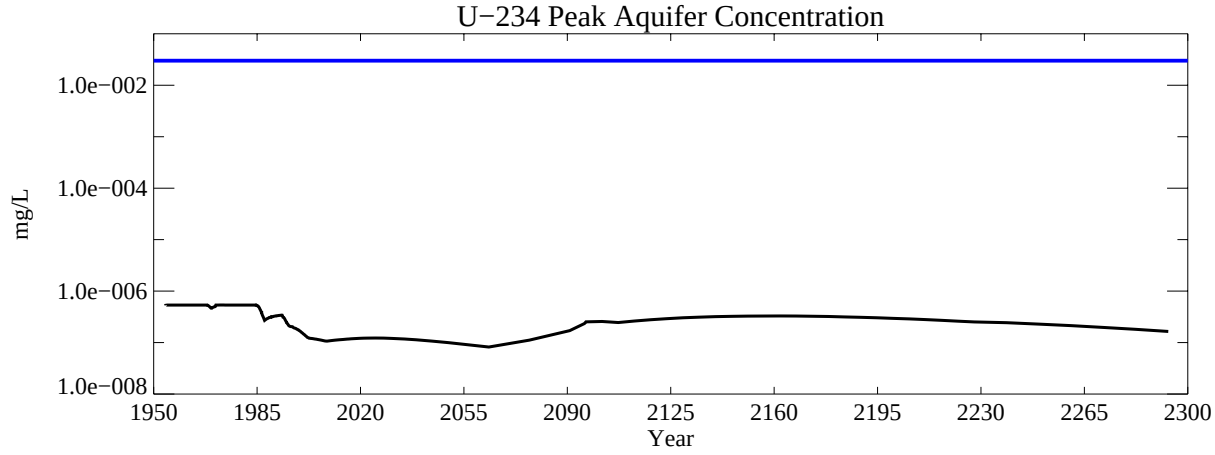

Figure A-9-38. U-234 peak aquifer concentrations (mg/L) (SRPA MCL = blue line, model predicted = black line).

A-9.3.8 Mercury

The sources of mercury in the vadose zone, listed in order of decreasing magnitude, are (1) the OU 3-13 soil sources at 585 kg, (2) the tank farm sources at 72.4 kg, (3) the failed CPP-3 injection well at 32.1 kg. The amount of mercury released directly to the aquifer due to the injection well failure was 368 kg.

A-9.3.8.1 Vadose Zone Mercury Simulation Results

Figures A-9-39 and A-9-40 illustrate the horizontal and vertical distribution of the vadose zone mercury at four time periods: 1979, 2005, 2049, and 2095. Figure A-9-41 presents the peak vadose zone concentrations through time and Figure A-9-42 illustrates the mercury mass arrival in the aquifer.

The peak vadose zone mercury concentration was 0.61 mg/L in 1990 and this date coincided with the start of OU 3-13 soil sources. A large amount of mercury was released to the INTEC vadose zone from the simulated tank farm releases and from the CPP-3 injection well failure. However, the sediment K_d (118 and 156 mL/g for the alluvium and interbed) results in the mercury moving very slowly through the vadose zone and allows the mercury to act as a continuous leaching source. The vast majority of the tank farm and OU 3-13 soil site mercury remains in the alluvium. The peak vadose zone concentrations are predicted to remain above the Snake River Plain Aquifer MCL through the end of the simulation period.

A-9.3.8.2 Aquifer Mercury Simulation Results

Figure A-9-43 illustrates the horizontal distribution the aquifer mercury at four time periods: 1979, 2005, 2049, and 2095. The peak aquifer concentration through time is presented in Figure A-9-44. The peak aquifer concentration was 9.67e-3 mg/L in 1981 and coincided with closing the CPP-3 injection well. Mercury concentrations were predicted to exceed the Snake River Plain Aquifer MCL from 1954 through 1993. The large alluvium and interbed K_d (118 and 156 mL/g) resulted in the mercury moving very slowly through the vadose zone. The peak aquifer concentration as a result of the vadose zone sources was 0.00016 mg/L in the year 3049.

Figure A-9-39. Mercury horizontal vadose zone concentrations (mg/L) (SRPA MCL = thick red line, 10*SRPA MCL = thin red line, SRPA MCL/10 = thin black line).

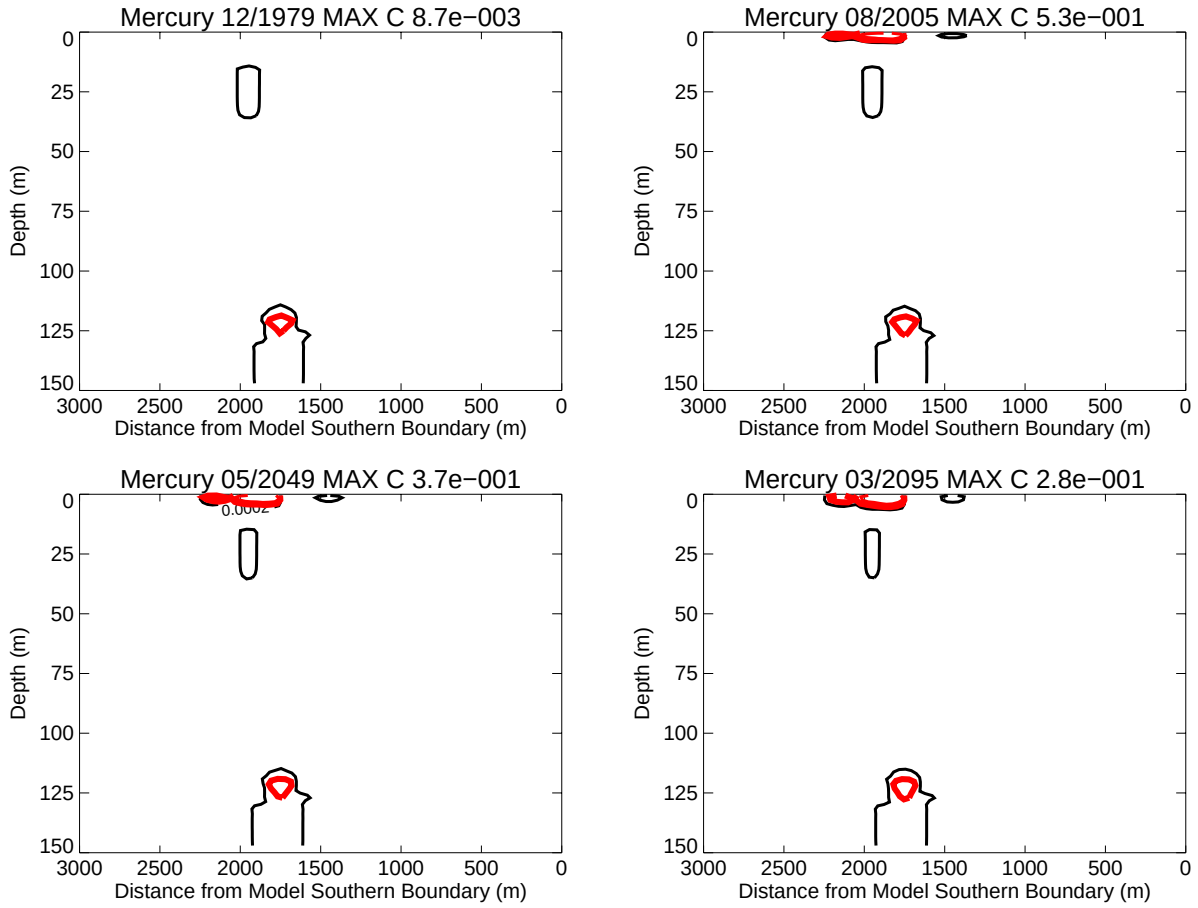

Figure A-9-40. Mercury vertical vadose zone concentrations (mg/L) (SRPA MCL = thick red line, 10*SRPA MCL = thin red line, SRPA MCL/10 = thin black line).

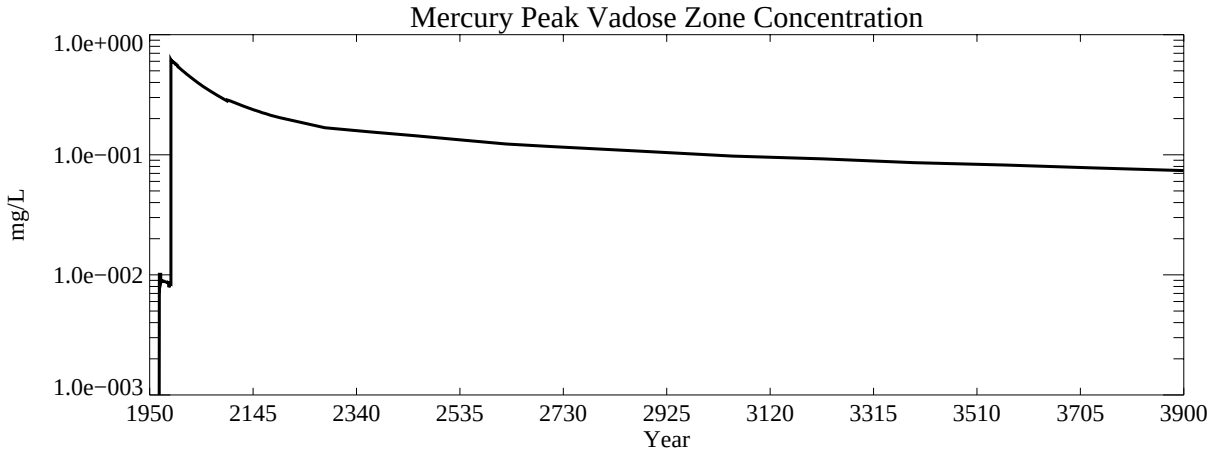

Figure A-9-41. Mercury peak vadose zone concentrations excluding tank farm submodel area (mg/L).

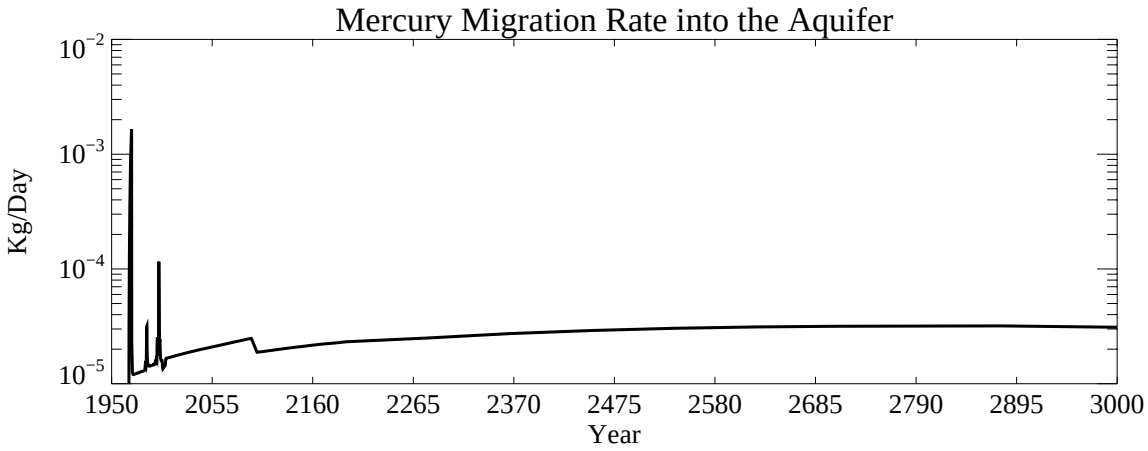

Figure A-9-42. Mercury mass flux into the aquifer (kg/day).

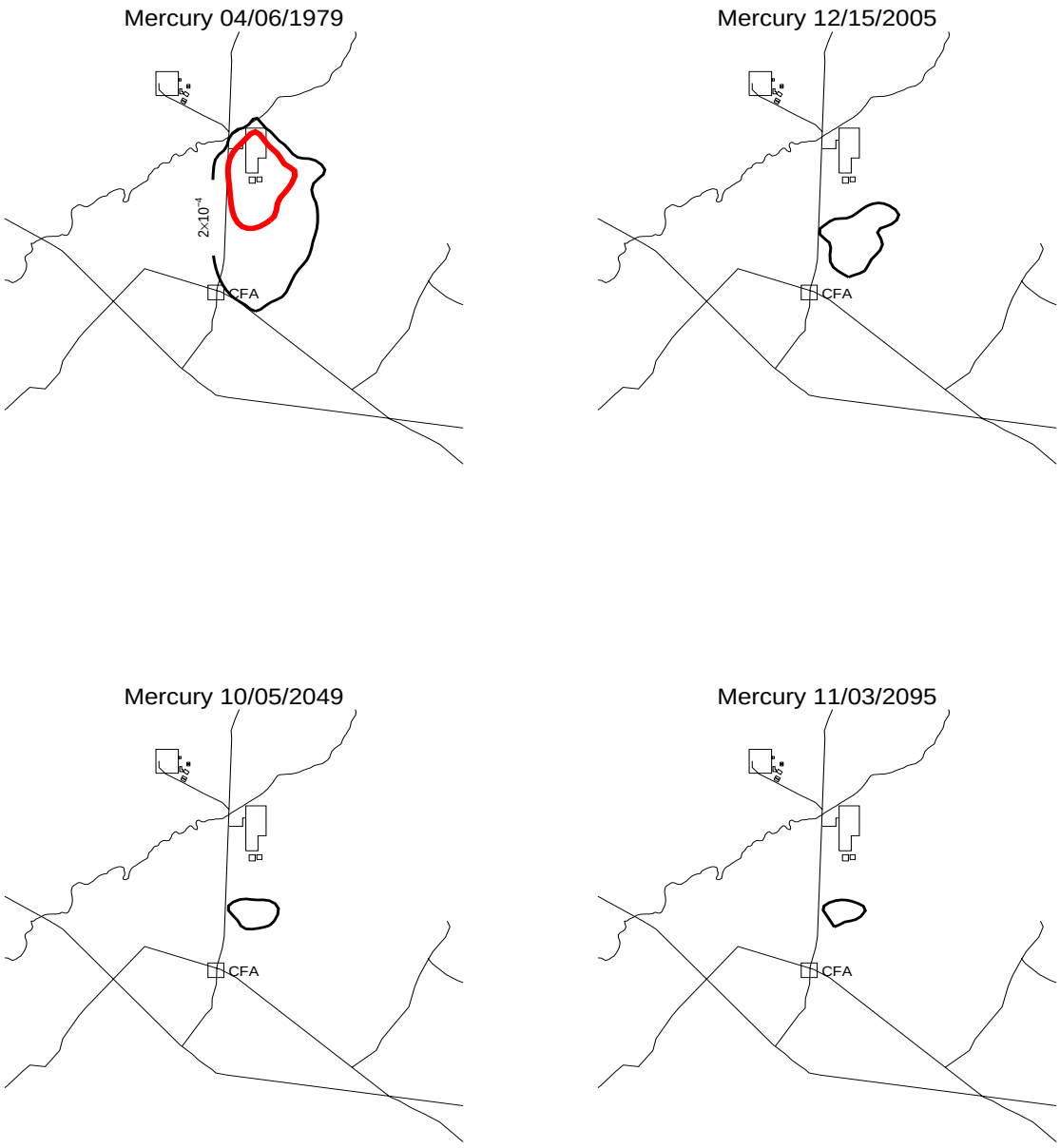

Figure A-9-43. Mercury horizontal aquifer concentrations (mg/L) (SRPA MCL = thick red line, 10*SRPA MCL = thin red line, SRPA MCL/10 = thin black line, SRPA MCL/100 = thin black dashed line).

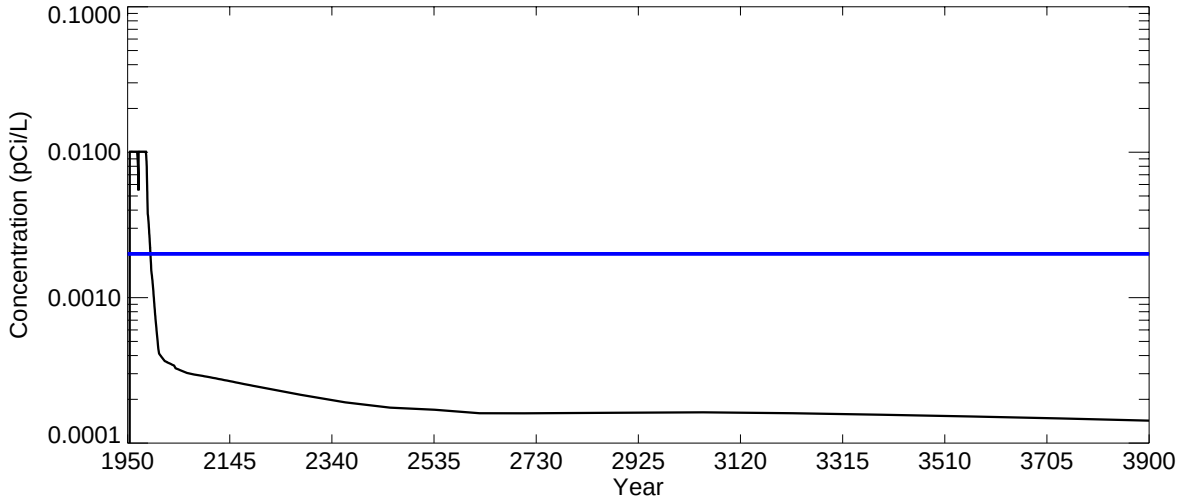

Figure A-9-44. Mercury peak aquifer concentrations (mg/L) (SRPA MCL = blue line, model predicted = black line).

A-9.3.9 Nitrate

The sources of nitrate in the vadose zone, listed in order of decreasing magnitude, are (1) service waste ponds at 1.3e+6 kg, (2) CPP-3 injection well failure at 2.2e+5 kg, and (3) the tank farm sources at 2.1e+4 kg. The nitrate released directly to the aquifer from the injection well was 2.6e+6 kg.

A-9.3.9.1 Vadose Zone Nitrate Simulation Results

Figures A-9-45 and A-9-46 illustrate the horizontal and vertical distribution of the vadose zone nitrate at four time periods: 1979, 2005, 2049, and 2095. Figure A-9-47 presents the peak vadose zone concentrations through, time and Figure A-9-48 illustrates the nitrate mass arrival in the aquifer.

The spent nuclear fuel reprocessed at the INTEC was dissolved in nitric or hydrofluric acid during the uranium recovery process, resulting in large amounts of nitrate discharged in the liquid waste. Nitrate is an anion and is very mobile in the subsurface. Nitrate is also ubiquitous in most groundwaters, and the background concentration in the Snake River Plain Aquifer is approximately 1.5 mg/L (Orr et al. 1991). The peak vadose zone concentration was 6.76e+2 mg/L after the 1972 CPP-31 release.

A-9.3.9.2 Aquifer Nitrate Simulation Results

Figure A-9-49 illustrates the horizontal distribution of nitrate in the aquifer at four time periods: 1979, 2005, 2049, and 2095. Figure A-9-50 presents the peak aquifer concentrations through time.

The peak aquifer nitrate concentration was 18.2 mg/L as N in 1993. A large amount of nitrate was present in both the injection well and service waste pond disposal water. The peak concentration corresponds to the combined input of both these sources to the aquifer. Nitrate was predicted to remain above the Snake River Plain Aquifer MCL from 1954 through 1998.

Figure A-9-45. Nitrate horizontal vadose zone concentrations (mg/L as N) (SRPA MCL = thick red line, 10*SRPA MCL = thin red line, SRPA MCL/10 = thin black line).

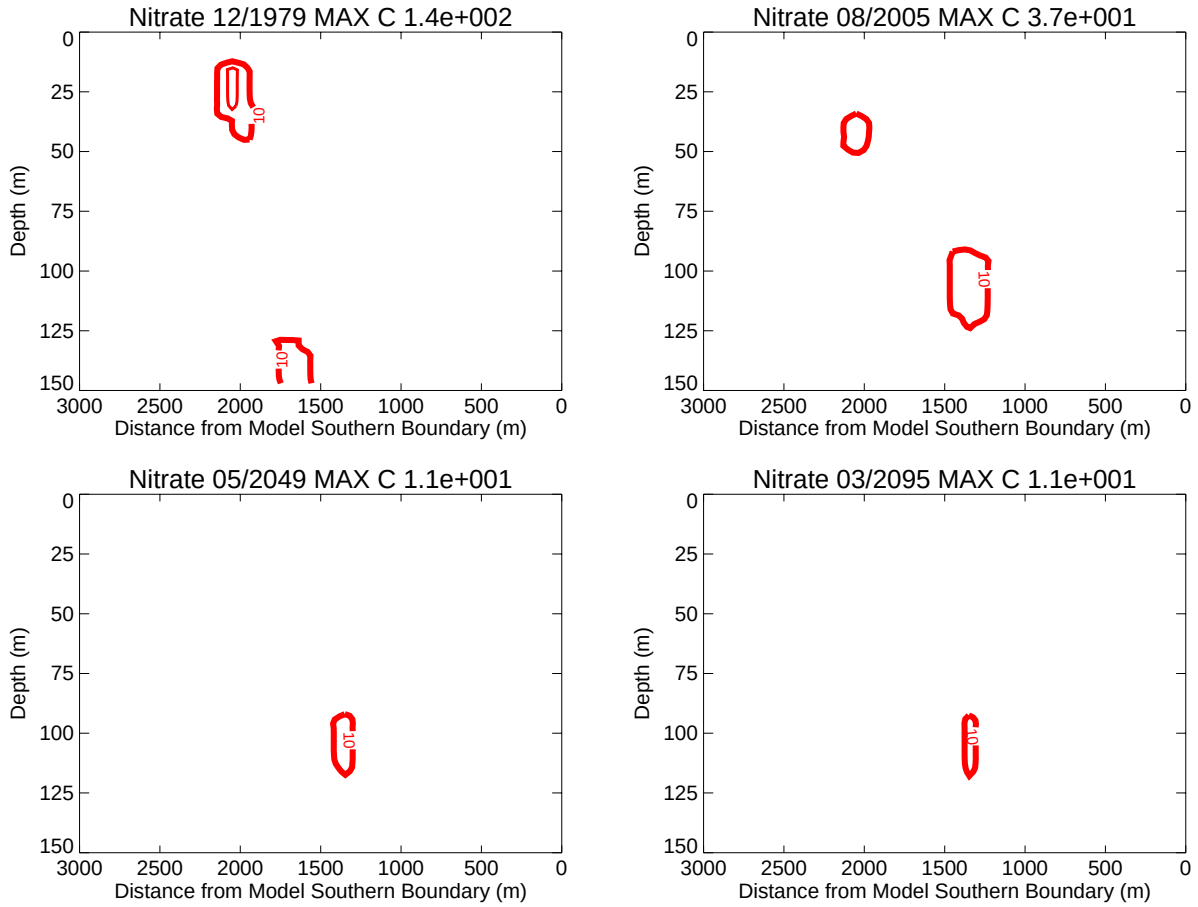

Figure A-9-46. Nitrate vertical vadose zone concentrations (mg/L as N) (SRPA MCL = thick red line, 10*SRPA MCL = thin red line, SRPA MCL/10 = dotted line).

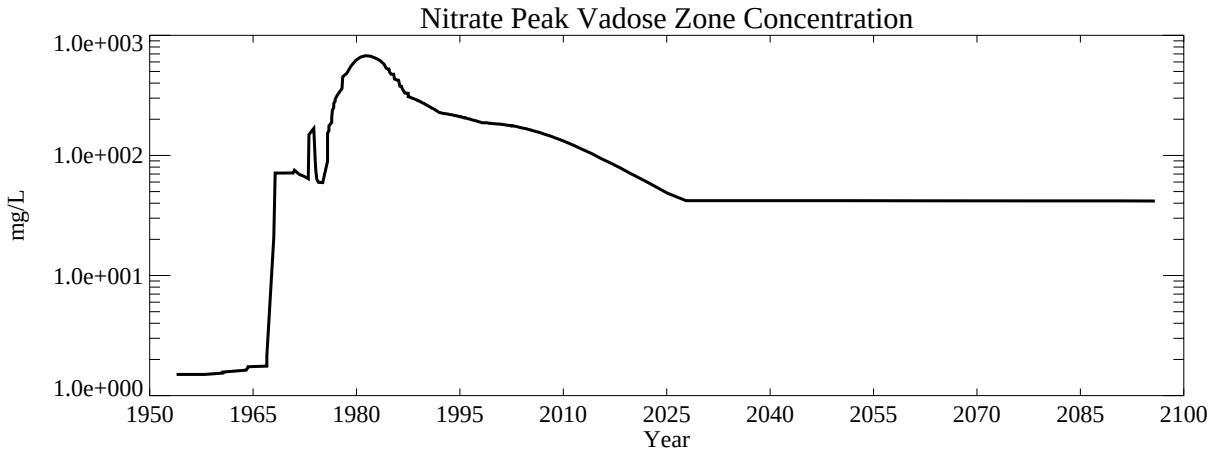

Figure A-9-47. Nitrate peak vadose zone concentrations excluding tank farm submodel area (mg/L as N).

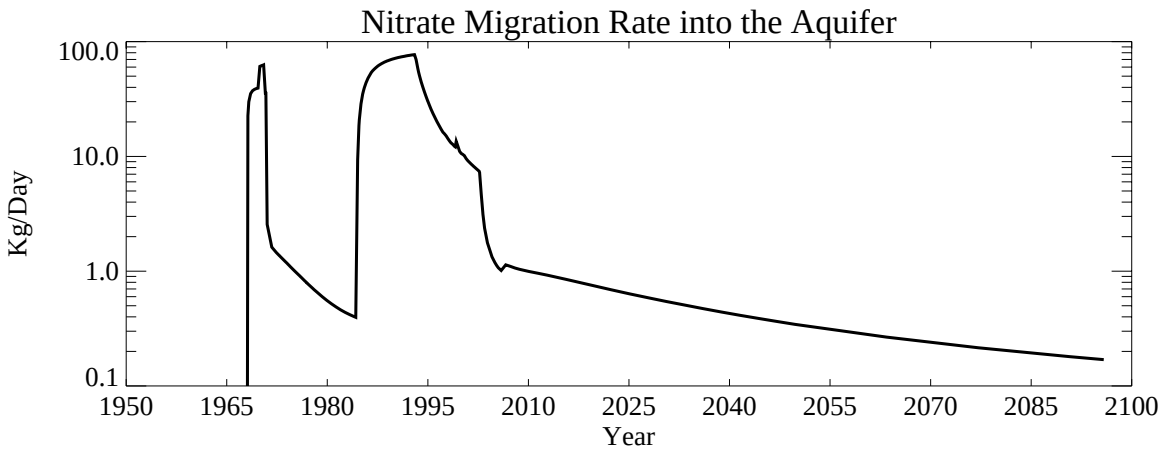

Figure A-9-48. Nitrate aquifer mass concentration history (kg/day as N).

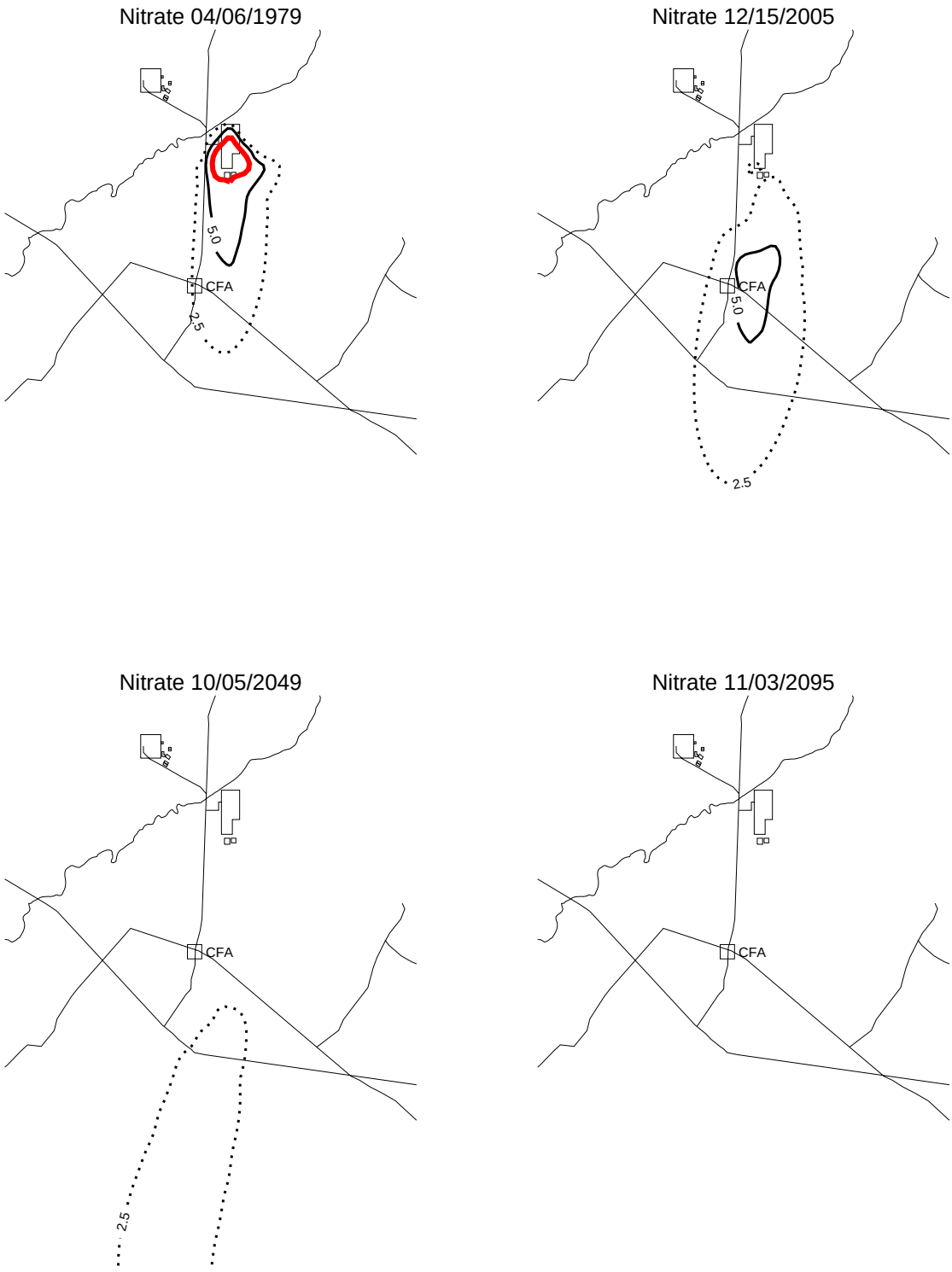

Figure A-9-49. Nitrate horizontal aquifer concentrations (mg/L as N) (SRPA MCL = thick red line, 10*SRPA MCL = thin red line, SRPA MCL/2 = thin black line, SRPA MCL/4 = thin black dashed line).

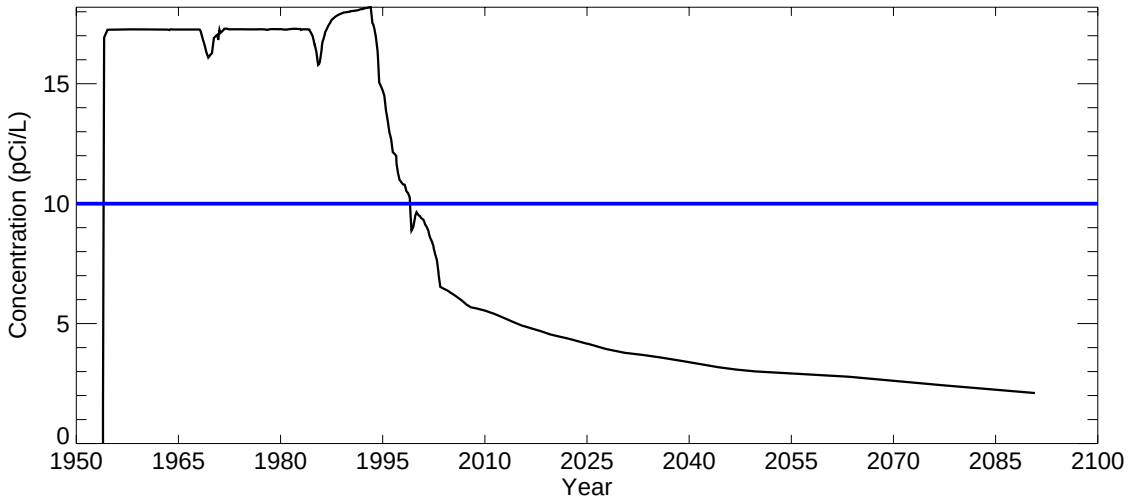

Figure A-9-50. Nitrate peak aquifer concentrations (mg/L as N) (SRPA MCL = blue line, model predicted = black line).

A-9.3.10 Groundwater Pathway Simulation Results Summary

The transport of 10 COPCs originating from the INTEC contaminated soil, CPP-3 injection well, and service waste ponds was simulated from land surface to the Snake River Plain Aquifer. The simulations also included contributing sources from the nontank farm OU 3-13 contamination sites. The simulation results are summarized for the vadose zone and aquifer in Sections A-9.3.10.1 and A-9.3.10.2, respectively. The Sr-90 simulation results are disscussed in Appendix J.

A-9.3.10.1 Vadose Zone Results

Table A-9-11 contains the simulated peak concentrations in the vadose zone model and includes the Snake River Plain Aquifer MCL, year of the peak concentration, peak concentration, peak concentration in 2005, peak concentration in 2095, and the year peak concentrations fall below the Snake River Plain Aquifer MCL. All the contaminants in the vadose zone except U-234 exceeded the Snake River Plain Aquifer MCL within the vadose zone at some time during the simulations. Only tritium and U-234 in the vadose zone were below the Snake River Plain Aquifer MCL before the year 2095. The timeframes over which vadose concentrations exceed the MCL are presented for reference only. The time when vadose zone concentrations fall below the Snake River Plain MCL provides an extremely conservative estimate of when the vadose zone pore water could not adversely impact the Snake River Plain Aquifer under any circumstance (i.e., fast flow paths and leaky well bores, etc.). Dispersion, dilution, adsorption, and radioactive decay within the vadose zone will result in aquifer concentrations being much less than those in the vadose zone.

Table A-9-11 Vadose zone simulation results.

COPC	SRPA MCL (pCi/L or mg/L)	Year of Simulated Peak	Peak Simulated Vadose Zone Concentration (pCi/L or mg/L)	Peak Simulated Vadose Zone Concentration in 2005 (pCi/L or mg/L)	Maximum Simulated Vadose Zone Concentration in 2095 (pCi/L or mg/L)	Year Below SRPA MCL in the Vadose Zone
H-3	20,000	1965	1.82e+6	3.13e+4	1.82e+2	2011
I-129	1	1971	3.00e+1	9.86e+0	3.37e+0	>2095[a]
Np-237	15	1990	6.00e+3	1.01e+3	2.88e+2	>2300[a]
Pu-239	15	1973	5.38e+1	1.01e+2	9.12e+1	14226
Pu-240	15	1990	1.94e+1	1.91e+1	1.71e+1	2287
Sr-90	8	1977	1.99e+9	1.94e+7	3.07e+4	>2300[a]
Tc-99	900	1982	1.64e+5	1.91e+4	1.68e+3	>2095[a]
U-234	0.03 (mg/L)	1990	8.27e-4	4.65e-4	1.47e-4	>2300[a]
Mercury	0.002	1990	6.14e-1	5.31e-1	2.81e-1	>4580[a]
Nitrate	10	1981	6.76e+2	1.61e+2	4.14e+1	>2095[a]
a. Concentration remained above Snake River Plain Aquifer MCL at simulation end time.						

A-9.3.10.2 Aquifer Results

Table A-9-12 contains the simulated peak concentrations in the aquifer model and includes the Snake River Plain Aquifer MCL, year of the peak concentration, peak concentration, peak concentration in 2005, peak concentration in 2095 and the year concentrations fall below the Snake River Plain Aquifer MCL.

Tritium, I-129, Np-237, Sr-90, Tc-99, mercury, and nitrate were predicted to exceed the groundwater Snake River Plain Aquifer MCL during the simulation time periods. However, only Sr-90 was predicted to exceed the Snake River Plain Aquifer MCL in the year 2095. The contaminants exceeding the Snake River Plain Aquifer MCL are summarized below:

- Tritium was predicted to exceed the Snake River Plain Aquifer MCL from 1954 through 2001. The primary source of aquifer contamination was the CPP-3 injection well prior to1984 and the service waste ponds after 1984. Radioactive decay, dispersion, and dilution reduce the tritium concentrations below the Snake River Plain Aquifer MCL by 2006. This is consistent with observed tritium concentrations in the aquifer monitoring wells.

- I-129 was predicted to exceed the Snake River Plain Aquifer MCL from 1954 through 2080. The primary source of aquifer contamination was the CPP-3 injection well and the service waste ponds. Dispersion and dilution reduced the I-129 concentrations below the Snake River Plain Aquifer MCL in the year 2088. Radioactive decay is negligible because the I-129 half-life is 1.57e+7 years. The simulated I-129 concentrations were consistent with the observed I-129 concentrations in the aquifer.

- Np-237 was predicted to exceed the Snake River Plain Aquifer MCL from 1954 through 1987. The

primary source of aquifer contamination was the injection well.

- Sr-90 was predicted to exceed the Snake River Plain Aquifer MCL from 1958 through 2128. The Sr-90 aquifer simulations are discussed in Appendix J.

- Tc-99 was predicted to exceed the Snake River Plain Aquifer MCL in 1999. The Tc-99 only briefly exceeded the Snake River Plain Aquifer MCL following the peak Big Lost River flow. This is the result of the tank farm Tc-99 residing deep in the vadose zone being quickly moved to the aquifer by the peak Big Lost River flow. Current aquifer concentrations exceed the Snake River Plain Aquifer MCL in the ICPP-MON-A-230 well and are approximately an order of magnitude higher than the simulated current highest aquifer concentrations. The recently drilled ICPP-2020 and -2021 wells confirm the ICPP-MON-A-230 well is not an anomaly, and a large area of the aquifer beneath INTEC is currently above the Snake River Plain Aquifer MCL. This suggests the vadose zone model may be overestimating vadose zone attenuation or underestimating the vadose zone Tc-99 sources. The Tc-99 source term for site CPP-31 has a greater uncertainty than the other radionuclides because the concentration was not measured during tank sampling but was estimated based upon fission yield. The accuracy of the Tc-99 inventory is likely only within a factor of two. Doubling the Tc-99 Site CPP-31 inventory would place the maximum simulated aquifer concentration (1999) near that currently measured in the aquifer. The simulated peak aquifer concentration in 2095 was approximately 10 pCi/L. This represents a factor of 100 decrease in concentration from simulated peak values. If the model trend is correct, concentrations should be nearly a factor of 10 below the Snake River Plain Aquifer MCL even if the inventory is increased by a factor of 10.

- Mercury was predicted to exceed the Snake River Plain Aquifer MCL from 1954 through 1993. The primary source of aquifer contamination was the CPP-3 injection well. Dispersion and dilution reduced aquifer concentrations below the Snake River Plain Aquifer MCL by the year 1994.

- Nitrate was predicted to exceed the Snake River Plain Aquifer MCL from 1954 through 1998. The primary source of aquifer contamination was initially the CPP-3 injection well and later the service waste ponds. The model predicts dispersion and dilution will reduce aquifer concentrations below the Snake River Plain Aquifer MCL by the year 1999. The simulated nitrate concentrations were consistent with the observed nitrate concentrations in the aquifer.

Table A-9-12 Aquifer simulation results.

COPC	SRPA MCL (pCi/L or mg/L)	Year of Simulated Peak	Peak Simulated Concentration (pCi/L or mg/L)	Maximum Simulated Concentration in 2005 (pCi/L or mg/L)	Peak Simulated Concentration in 2095 (pCi/L or mg/L)	Year Below SRPA MCL
H-3	20,000	1965	4.02e+6	9.97e+4	1.23e+2	2001
I-129	1	1970	2.26e+1	3.85e+0	9.00e-1	2080
Np-237	15	1965	2.71e+1	4.06e+0	4.22e+0	1987
Pu-239	15	1960	3.34e-1	1.72e-2	2.07e-3	Always
Pu-240	15	1960	1.67e-1	8.61e-3	1.03e-3	Always
Sr-90	8	1965	5.76e+3	4.08e+1	1.81e+1	2128
Tc-99	900	1999	9.35e+2	2.35e+2	9.84e+0	1999
U-234	0.03 (mg/L)	1958	5.36e-7	1.15e-7	2.34e-7	Always
Mercury	0.002	1981	9.67e-3	5.86e-4	1.30e-4	1993
Nitrate	10	1993	1.82e+1	6.20e+0	2.10e+0	1998

A-10 ASSESSMENT OF MODEL LIMITATIONS

The models used in this analysis are simplified representations of the vadose zone and aquifer. Mismatches between measured data and predictions arise as a result of simplified parameterization and uncertainty in input parameters. The sensitivity and uncertainty in predictions are quantified and bounded in the following sections. The model sensitivity was assessed by determining the potential range of model output given natural variability in the input parameters. This is done and to determine whether the possible range of each parameter value can result in significant variation in model predictions. The model sensitivity to parametric variability is presented in Section A-10.1.

Predictive sensitivity can be quantified using Monte Carlo simulation given the probability density of each parameter and given the joint density between parameters. In Monte Carlo simulation, repeated random sampling from each probability distribution is used in forward simulations, and the resultant of many such simulations is a distribution of possible model predictions. In these simulations, there are insufficient data from which to determine the probability density (and joint density) functions for each parameter (or each combination of parameters). As a result, model parametric uncertainty is qualitatively evaluated based on the behavior of selected sensitivities.

Each predictive simulation is subject to both parametric uncertainty and conceptual uncertainty. The conceptual uncertainty is in addition to the parametric variability captured in the sensitivity analysis. This uncertainty arises through the development of the conceptual model of flow and transport because complex processes may be oversimplified or poorly understood. It is introduced as the contaminant source releases are estimated and is compounded as transport parameters and boundary conditions are assigned. The relative impact of these sources of uncertainty is qualitatively discussed in Section A-10.2.

A-10.1 Model Sensitivity Analysis

Model sensitivity, or the relationship between information being input and output, is presented in this section for a select set of model inputs. This sensitivity analysis can be used to focus the uncertainty analysis, i.e., only those model inputs resulting in large deviations in model output require discussion in the model uncertainty analysis. The model calibration process reduces the initial uncertainty by seeking to obtain a match between observed and predicted conditions. The subsurface underlying INTEC is complex, the boundary conditions are variable, and the data are not always located optimally in both space and time. As a combined result, there is a resultant mismatch between model predictions and observed data. The “uncertain” parameters are included here as the basis of the model sensitivity/uncertainty analysis. Seven model parameters or design features were identified as having a potentially large impact on model predictions during the model calibration work. The sensitive parameters are (1) the interbed structure and permeability, (2) assumed recharge from precipitation, (3) existence of fast flow paths allowing Tc-99 to reach the aquifer at the ICPP-MON-A-230 well, (4) the Tc-99 service waste source, (6) the horizontal discretization used in the model, and (7) strontium sorption and dispersion. The sensitivity investigation presented in this section focused on Tc-99. The Sr-90 model sensitivity hydrological inputs is presented with the geochemical modeling in Appendix J. The simulations testing the sensitivity to these parameters are listed in Table A-10-1, and the results are summarized in Section A-10.1.6.

Table A-10-1 Sensitivity analysis simulations.

Sensitivity Simulation	Section	Parameter values
Interbed thickness and permeability	A-10.1.1.1	Highest conductance for Tc-99
	A-10.1.1.2	Lowest conductance for Tc-99
Alluvium recharge rate	A-10.1.2.1	3 cm/year tank farm recharge for Tc-99
	A-10.1.2.2	39 cm/year tank farm recharge for Tc-99
	A-10.1.2.3	Maximum possible recharge focused on the northern INTEC
Tc-99 preferential flow path between the 380-ft interbed and aquifer near the location of ICPP-MON-A-230	A-10.1.3.1	10 gal/min preferential flow path from 380 ft interbed
Tc-99 service waste inventory	A-10.1.4.1	Estimate from 25.1 Tc-99/I-129 ratio
Horizontal grid discretization	A-10.1.5.1	50- x 50-m horizontal grid for Tc-99

The base case simulations for the sensitivity analysis correspond to the Tc-99 calibration results discussed in Section A-7.3.1. Comparisons to the base case (calibration run) are presented by plotting the sensitivity run and base case values for peak concentrations (vadose zone and aquifer) and mass flux rates into the aquifer.

A-10.1.1 Interbed Thickness and Permeability

The contrast between basalt and sediment hydraulic and transport properties is large and their structural distribution is highly variable. Structural variability can change primary flow paths, allowing contaminants to bypass interbeds or to flow through sediment regions with higher permeability.

Spatial stochastic simulation based on variogram models for high- and low-permeability alluvium, interbed, and basalt were used to generate the structure used in the calibration and base case simulations. This process generates many realizations, each honoring the underlying statistical parameters. The calibration and baseline risk assessment simulations used the most probable (or average) structure as the basis of the predictions. To test the sensitivity of these structures, a highest conductance structure (i.e., minimum interbed thickness and maximum interbed permeability) and a lowest conductance structure (i.e., maximum interbed thickness and minimum interbed permeability) were selected from the realizations. The most conductive structure defined 10% of the subsurface as interbed with 5% being low-permeability interbed. The least conductive structure defined 15% of subsurface as interbed with 10% being low-permeability interbed. The model calibration simulation and base case sensitivity simulation had 14% as interbed with 8% being low-permeability interbed.

The highest conductance simulations resulted in fewer areas of high saturation and much less perched water beneath the Big Lost River than was predicted in the base case. The lowest conductance simulations resulted in more areas of high saturation but did not significantly increase the areal extent of the perched water beneath the Big Lost River from the base case. However, the location of the perched water was slightly different from the base case. Figures A-10-1 and A-10-2 illustrate the horizontal extent of perched water in the INTEC subsurface for the highest and lowest conductance simulations, respectively. These figures can be compared to the base case perched water locations contained in Figure A-7-1.

These structures were used as the basis of Tc-99 transport simulations in combination with the base case inventories to evaluate transport sensitivity. The results of these two simulations are presented in Sections A-10.1.1.1 and A-10.1.2.

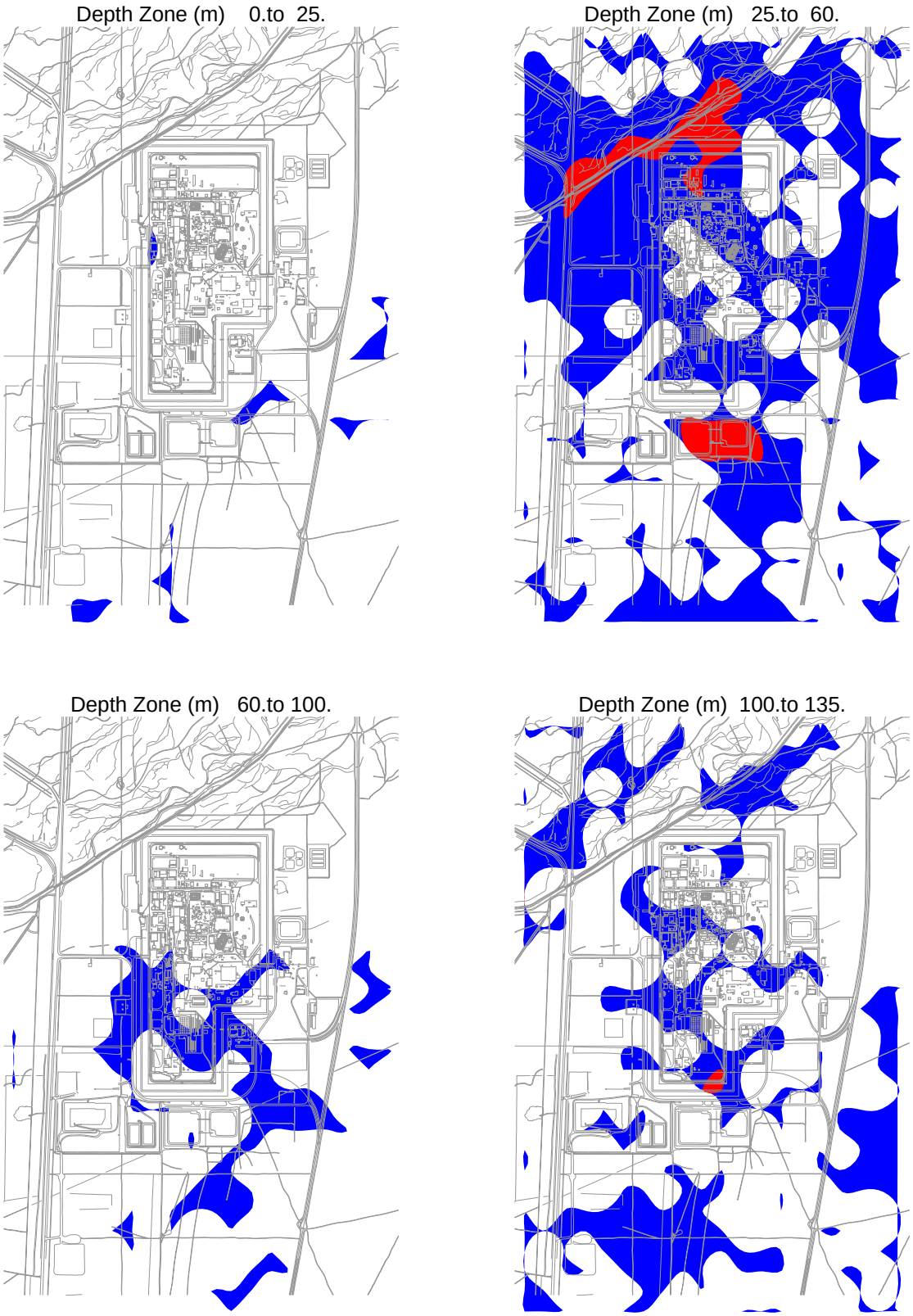

Figure A-10-1. Highest interbed conductance simulation horizontal extent of simulated perched water during peak Big Lost River flow (1999) (blue = 0.99 saturation, red = 1.0 saturation).

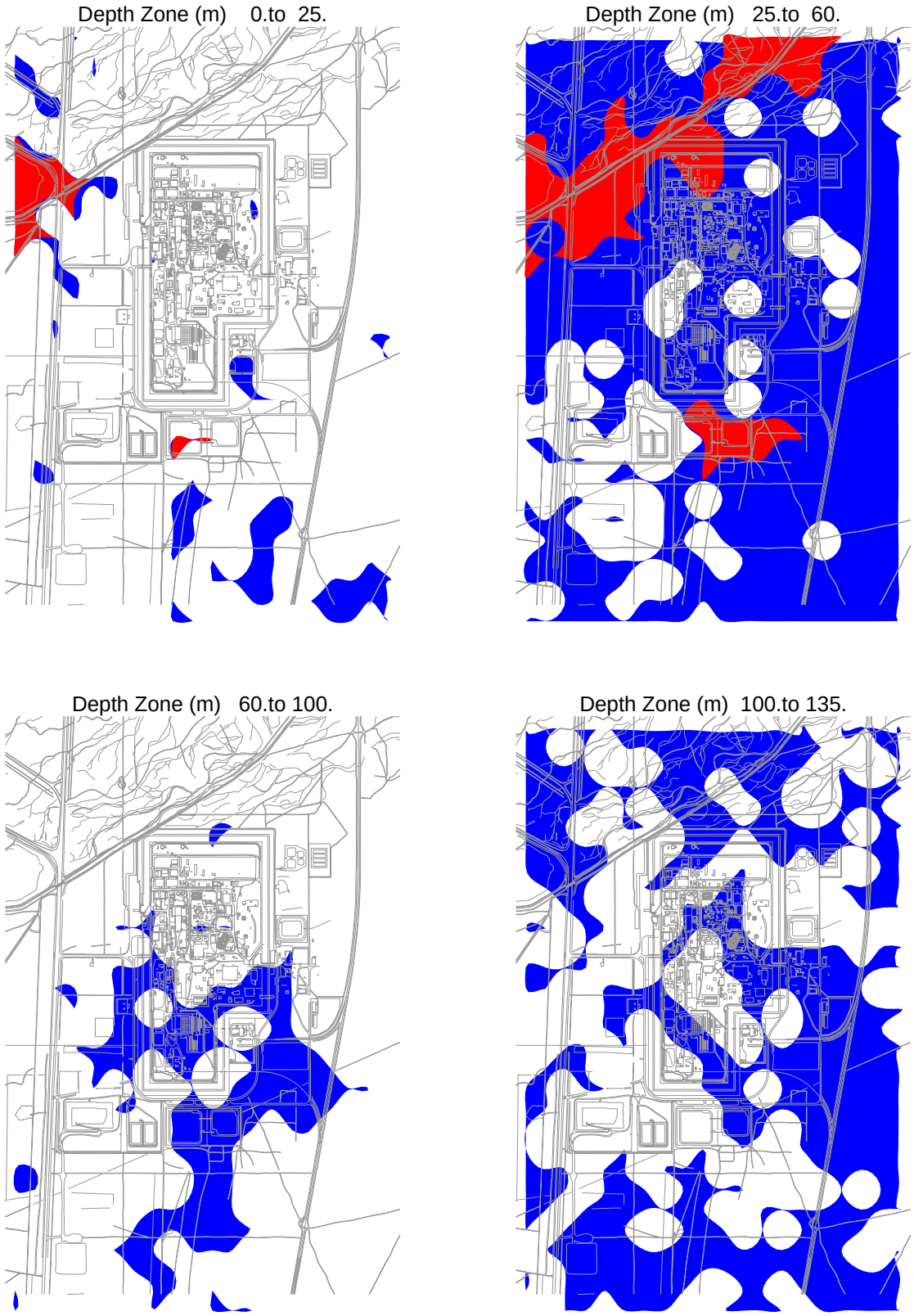

Figure A-10-2. Lowest interbed conductance simulation horizontal extent of simulated perched water during peak Big Lost River flow (1999) (blue = 0.99 saturation, red = 1.0 saturation).

A-10.1.1.1 Highest Interbed Conductance for Tc-99

The peak simulated concentration in the vadose zone for this case is 1.65e+5 pCi/L in 1978, which is after the CPP-31 release date. The peak concentration declined to 1.91e+4 pCi/L in 2005 and to 1.68e+3 pCi/L in 2095. Figures A-10-3 and A-10-4 illustrate the vertical and lateral extent of the simulated vadose zone concentrations. The shallow vadose zone contamination located immediately northwest of the former percolation ponds is due to the CPP-22 OU 3-13 soil site (0.1 Ci), which was placed in the model in 1990.

Figure A-10-5 illustrates the peak simulated vadose zone concentration through time and is the peak concentration anywhere within the vadose zone model domain. The peak vadose zone concentration falls below the MCL in approximately the year 2095. The Tc-99 activity flux into the aquifer is illustrated in Figure A-10-6 and is the total activity passing from the vadose zone model to the aquifer model. Four peak activity periods can be seen in Figure A-10-6. These are the result of the following: (1) the injection well failure during the late 1960s, (2) the service waste ponds during the early 1980s to the early 1990s, (3) the transient Big Lost River recharge during the late 1990s, and (4) the long-term average Big Lost River recharge following the recent hydrologic drought.

Figure A-10-6 indicates that the fluctuations caused by the historical Big Lost River flows are less than the base case because thinner and higher-permeability interbeds do not allow the Big Lost River water to move far enough laterally to reach the contaminated area beneath the tank farm. In addition to the effect of increased average interbed permeability, the surface slope of the 140-ft interbed was different in the maximum interbed realization of the vadose zone lithology. The dip towards the tank farm was less severe. The resultant transport through the vadose zone is controlled by the relatively constant anthropogenic and precipitation recharge. The Tc-99 concentration in key perched water wells is illustrated in Figure A-10-7. The overall agreement with the observed perched water concentration is similar to the base case.

Figure A-10-8 illustrates the horizontal aquifer concentrations and Figure A-10-9 illustrates peak aquifer concentrations through time. The peak concentration is taken from anywhere within the model domain and is at the CPP-3 injection screen during injection well operation or is at the water table for vadose zone sources percolating into the aquifer. Several distinct changes in peak groundwater concentration can be seen in Figure A-10-7. These are the result of the following: (1) service waste disposed in the CPP-3 injection well prior to 1968, (2) service waste entering the aquifer from the vadose zone during the well failure period, (3) service waste disposed of in the CPP-3 injection well after repairs in 1970, (4) service waste intermittently disposed of in the CPP-3 injection well after the service ponds began operating 1984, (5) service waste from the pond operation entering from the vadose zone after 1984, and (5) tank farm contamination entering from the vadose zone during high Big Lost River flow years in the late 1990s. Records of water volume and Tc-99 activity disposed of to the CPP-3 injection well after 1984 indicate widely varying contaminant concentrations in the well influent.

The abrupt increases in aquifer concentrations during peak Big Lost River flow years are not apparent in the minimum interbed thickness peak aquifer concentrations. This is because the Big Lost River does not spread laterally beneath the tank farm to the same extent as the base case. The peak simulated aquifer concentration in 2095 was 43 pCi/L and was four times higher than the base case. This is because the Big Lost River has less of an effect in quickly moving contaminants into the aquifer in the base case.